Long range dispersal and spatial pattern formation in biological invasions

Sergio A. Cannas [a,b,*], Diana E. Marco [b,c], Marcelo A. Montemurro [d]

[a] *Facultad de Matemática, Astronomía y Física, Universidad Nacional de Córdoba,*
Ciudad Universitaria, 5000 Córdoba, Argentina
[b] *Member of National Research Council (CONICET), Argentina*
[c] *IIB-INTECH, Camino Circunvalación, Laguna Km 6. CC 164 (7130), Chascomús, Buenos Aires, Argentina*
[d] *Faculty of Life Sciences, Moffat Building, P.O. Box 88, University of Manchester,*
Manchester M60 QD, United Kingdom

Abstract

In this paper we explore the consequences of long distance dispersal in biological invasion processes through simulations using a recently developed cellular automaton model. We show that long distance dispersal generate characteristic spatial patterns with several stationary scale-invariant properties. In particular, the patterns display a main patch around the focus of spread, with a fractal border structure whose fractal dimension contains information about the main statistical properties of the dispersal mechanism. Our results are in agreement with field data of spread of invaders with long distance dispersal mechanisms.
© 2006 Elsevier Inc. All rights reserved.

Keywords: Biological invasions; Cellular automata; Long-distance dispersal

---

* Corresponding author. Fax: +54 351 4334054.
  E-mail address: cannas@famaf.unc.edu.ar (S.A. Cannas).

1. Introduction

Events of long-distance dispersal (LDD) are increasingly recognized as the main factor involved in global and fast paleocolonization of terrestrial habitats [1,2], pathogen dispersal by air and water [3,4], and biological invasions more related to human influence [5–7]. The shape of the dispersal function underlying these common events is of paramount importance to understand the temporal and spatial patterns of organisms spread. Attempts to fit observed dispersal distributions have been mostly driven by the usage of the negative exponential functions, although in recent years it has been recognized that functions like the power law are more suitable to account for occurrence of unusual, extreme dispersal events [8,9]. It is well known that power law dispersal distributions of crop pathogens generate a particular spatial pattern of spread, characterized by the absence of well-defined epidemic fronts [8], and the generation of clusters of different sizes [10]. However, in our knowledge no attempt has been done to characterize the spatial pattern of spread of these pathogens with more detail. The same kind of spatial patterns can be expected to be generated during the dispersal of invaders into new habitats if LDD events are involved. This paper examines these spatial patterns using a cellular automaton model previously developed for the study of biological invasions [11,12]. In this paper we found that these patterns are characterized by different scale-invariant properties. That means, not only self-similar or fractal geometrical characterizations [13], but also power law behavior of different statistical distributions. Power law behavior is now recognized ubiquitous in nature and reflects the invariance of some property over some range of temporal and spatial scales. The scale invariant properties we found are consistent with field data of spread of invaders with long-distance dispersal mechanisms. These properties are also common to other physical systems with long range interactions [15–17].

2. The model

To analyze the influence of LDD strategies on an invasion process we used a spatially explicit individual-based model. This model is a particular case of a recently developed cellular automaton, called an Interacting Multiple Cellular Automata (IMCA) [11,12], which allows to consider several interacting species, taking into account the life history traits of the involved species relevant to species' dynamics [12]. In order to separate the effects derived from the proper long range dispersal strategies of invaders from those related to interactions with the natives, we consider in this work the particular case of the spread of only one isolated species (the invader) in a clean open field, keeping just the interacting rules between individuals of a single species of the IMCA. In other words, we consider the case where interactions with other species can be neglected. We briefly summarize now the characteristics of the model.

The model is embedded on a square grid containing $L_x \times L_y$ cells, representing the field. For a single species the model associates to every cell i in the grid a discrete variable $a_i(t)$ which encodes the age of an individual located at it at time t; $a_i = 0$ corresponds to an empty cell [12]. The index i encodes a pair of discrete coordinates (x, y), with $x = 1, 2, \ldots, L_x$, $y = 1, 2, \ldots, L_y$. The grid parameter (i.e., the distance between neighboring cells) equals one. The spatial length scale is chosen so that each cell contains at most one adult individual. The dynamical variables are updated according to a parallel dynamics, that is, the value of all variables at a given (discrete) time t depends on

the value of the variables at time $t - 1$. The time scale is chosen to coincide with the minimal reproductive interval in the life history of the species, settled as one year for plant species. Life history traits included are: d, mean seed dispersal distance (in grid units), q, annual adult survival probability, t_m, age of reproductive maturity (in years), n, mean seed production (seeds/plant), t_s, interval between masting seed crops (in years), f_g, mean germination probability and P_s, juvenile survival probability [12].

An occupied site $a_i(t) \neq 0$ is updated according to the following rule [12]:

$$a_i(t + 1) = \begin{cases} a_i(t) + 1 & \text{with probability } q \\ 0 & \text{with probability } 1 - q \end{cases} \tag{1}$$

where q is the annual *adult survival probability*. Now consider an empty cell i at time $t - 1$, that is, $a_i(t - 1) = 0$. The site will be colonized at time t, that is, $a_i(t) = 1$ with a probability $p_i(t)$ given by [12]

$$p_i(t) = 1 - (1 - P_s f_g)^{s_i(t)} \tag{2}$$

where $s_i(t)$ is the number of seeds received by the cell i at time t; $p_i(t)$ is the probability that *at least* one seed germinates *and* that the corresponding individual survives to the adult stage (more than two years). s_i is obtained by counting the seeds received by the cell i coming from the rest of the cells. Seed dispersion of an individual is assumed isotropic and it is described by some density function $f(r)$, where $r = \sqrt{x^2 + y^2}$ is the distance to the parental tree. The function $f(r)$ describes the fraction of the total number of seeds produced by a single individual that are dispersed per unit of area to a distance r; $f(r)$ is assumed to be normalized in the whole plane. The number of seeds received by a cell j coming from an individual located at a cell i is then given by $n\, f(r_{ij})$ where r_{ij} is the distance between the center of the cells i and j. Then s_i is obtained by summing $n\, f(r_{ij})$ over all the cells j containing a mature tree [12].

Let us now analyze the dispersal distribution function $f(r)$. The difference between short and long range dispersal is related to whether or not the distribution $f(r)$ has an exponentially bounded tail [9]. In a very general sense this means that the distribution is *short ranged* if the moments $\int r^n f(r)\, da$ are finite for *every* value of $n \geqslant 0$, where the integral extends over the infinite plane; otherwise, it is long ranged [9]. An example of short range dispersal is given by the negative exponential function

$$f(r) = \frac{2}{\pi d^2} e^{-2r/d} \tag{3}$$

where $d = \int r f(r)\, da$ is the mean dispersal distance. This function has been shown to appropriately describe the dynamics of different invasion systems where all the species involved have short ranged dispersal strategies [11]. LDD mechanisms can be simulated by a power law function:

$$f(r) = \begin{cases} \frac{A}{r^\alpha} & \text{if } r \geqslant 1/2 \\ 0 & \text{if } 0 < r < 1/2 \end{cases} \tag{4}$$

where A is a normalization constant and $\alpha > 2$ (otherwise the density function f cannot be normalized). If we consider statistical averages of different dynamical quantities in the model, we expect three different type of behaviors, according to the values of α. When $3 < \alpha \leqslant 4$ the first moment

remains finite but the second moment becomes infinite. The mean dispersal distance is given by $d \equiv\ <r> = (\alpha-2)/2(\alpha-3)$. When $2 < \alpha \leqslant 3$ both first and second moments are infinite and the mean dispersal distance is not defined. Finally, for $\alpha > 4$ both the first and the second moments of the distribution are finite. Hence, even when the distribution is strictly long ranged, it can be well approximated by a normal distribution on finite spatial scales. So, no qualitative differences are expected in the global spatial pattern of spread between this case and the short range one. Several results for other physical systems with long ranged interactions support this assumption [16–18].

3. Methods

We performed numerical simulations using the model described in the previous section in order to determine the main features of the spatial pattern developed by a species with LDD during its spread. In almost all the simulations we considered the spread of an isolated species from a single focus, i.e., we started all our simulations with a single mature individual located a the center of a square area ($L_x = L_y = L$). The fact of considering the spread from a single focus is not restrictive and can be thought as representative of a starting situation with a localized distribution of individuals. Indeed, several simulation checks starting with a localized initial distribution like, for instance, a line of mature individuals at the border of a empty rectangular area, showed the same overall behavior.

The simplest implementation of the algorithm consists in checking for every grid site all the other sites that can send seeds to it at every time step (one year). While in the case of short range dispersal this procedure involves counting a limited number of sites (independent of L), it requires $\mathcal{O}(L^4)$ operations at every time step in order to update the whole population in the long range case (while it requires $\mathcal{O}(L^2)$ in the short range case). That is because each update of the L^2 sites would require checking the L^2-1 other sites to account for incoming seeds. Moreover, the need for continuous checking on the particular age range of the site being updated also poses further computational burden. In our computer code, instead of working with a two–dimensional array data structure we have implemented three dynamic lists of pointers to empty, young and mature sites, respectively. However, even this implementation considerable reduces the simulation time by eliminating unnecessary checks in the computations (the increase in speed for a typical simulation of a 1024×1024 system is close to a factor of 100 respect to the array-based implementation), it does not change the computational complexity of the algorithm. This is because every simulation run covers a time period (in system years) that runs up to the time needed by the system to completely fill the simulation area. At short times (compared with total simulation time) the size of the mature sites list is independent of the system size and the simulation speed is very high. But after a small quantity of reproductive periods (t_m) the exponential increase in the population of the mature sites becomes of the order of the total number of sites. Therefore, the main contribution to the number of computational operations needed in a single run is given by the latest stages in the simulation and it results again $\mathcal{O}(L^4)$ (although with a reduced prefactor respect to the array-based implementation). Most of the results presented in this work were calculated for a 1024×1024 system size. We performed also some checks for a 1500×1500 system size, but the results remained essentially unchanged.

Our analysis of the simulation results is based on the statistics of patches of occupied sites and their borders. The algorithmic structure used for patch extraction and border calculation is the following. At a fixed time occupied sites are assigned to patches by giving them a label, representing their corresponding patch number. The algorithm for patch extraction proceeds systematically by examining every site in the grid. When an unlabelled occupied site is found, the algorithm creates a new patch by assigning a new label to the current site and to all the connected set of occupied sites associated to it. More specifically, for each site currently in the patch all the occupied sites in the immediate neighborhood (the immediate neighborhood of a site is defined here as the set of 8 closest sites surrounding the current one) are assigned to the same patch. The algorithm continues recursively until no more sites are added to the current patch. Then, the next unlabelled site is considered, and the procedure is repeated until no unlabelled occupied sites are left. Finally, all the relevant information for patch statistics can be extracted from the table of labels. Once all the trees in the grid are assigned to patches, the border extraction is straightforward. A given occupied site is defined as lying at a patch border only if at least one of the sites in its immediate neighborhood is not occupied by a tree. Therefore, the border set of a given patch is simply defined as the list of all the occupied sites lying at its border.

Sensitivity analysis has shown that the dynamical behavior of averaged quantities (such as the population density and others) in the IMCA depends mainly on only two parameters [12]: the reproductive maturity t_m and the mean dispersal distance d (or the exponent α in the case of a dispersal distribution function of the form (4)). Hence, we chose a set of typical values [11] for the rest of the parameters and kept them fixed in all the simulations, namely, $q = 0.96$; $n = 14\,000$; $t_s = 1$; $P_s = 0.4$; $f_g = 0.2$.

We compared the simulation predictions with spatial patterns obtained from field data for two different species for which events of LDD appear to be dominant: *Cryptostegia grandiflora* and *Pinus ponderosa* (see Section 5).

We use an operational definition of invasive species, as a species that spreads in space, either occupying new habitats, or increasing its cover in areas previously occupied. This approach allows for a more general treatment of the invasion problem, since cases in which native species become invaders after some habitat or climatic change (for example, shrub encroachment [19]) can also be considered. Thus, although most of invasions are thought to be caused by non-native species, a key for distinction is between invasive or non-invasive species, rather than native or non-native species [20].

4. Numerical results

In order to illustrate the main qualitative differences between the behaviors obtained with the different dispersal strategies, we present in Fig. 1(a) comparison between the typical spatial patterns predicted by the IMCA for species with short and long range dispersal for a system size $L = 200$ and $t_m = 7$. In Fig. 1(a) we show a sequence of snapshots taken at different times during the same simulation run using the dispersal function Eq. (3) with $d = 5$; in Fig. 1(b) we show a sequence of snapshots taken at different times during a simulation run using the dispersal function Eq. (4) with *exactly* the same set of parameters as in Fig. 1(a) ($d = 5$ in this case corresponds to a value $\alpha = 3.11$). In the short range case the spatial spread produces a compact patch with a rough
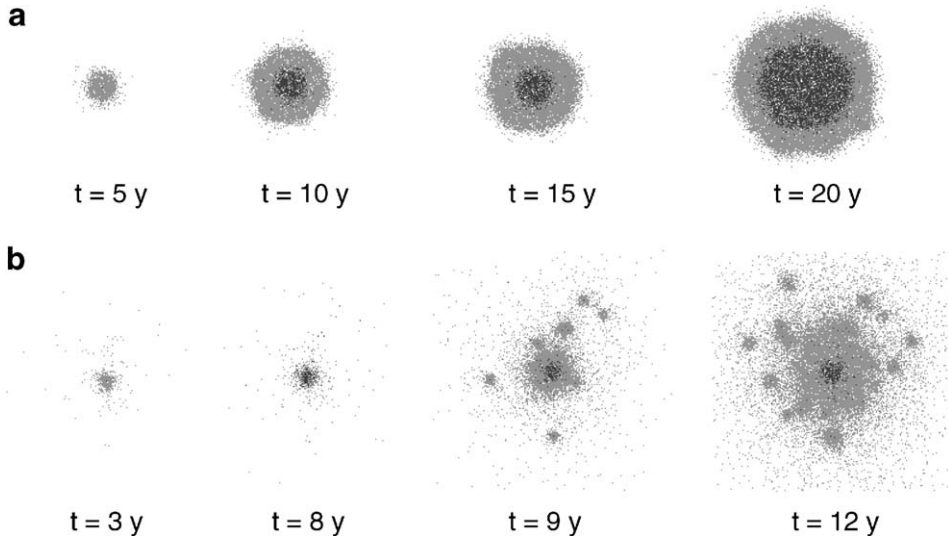
Fig. 1. Snapshots of the spread from a single focus at the centre of a square area with $L = 200$, $d = 5$ and $t_m = 7$, at different times. The dark points correspond to mature individuals while the light grey ones to non-mature individuals. The simulation starts with a mature individual at the focus. (a) Species with short range dispersal; (b) species with long range dispersal ($\alpha = 3.11\ldots$).

border of almost circular shape, surrounded by a few isolated individuals and very small patches. A numerical calculation of the average radius of the main patch (and hence the invasion front) shows that it increases at constant velocity, as expected for a system with short range dispersal [9] (the main patch is defined as the patch containing the largest number of sites; see section Methods for details of patch extraction algorithms details). On the other hand, the introduction of long range dispersal produces a dramatic change in the spatial distribution, where we can appreciate the development of a very structured and complex pattern. Such behavior can be easily understood as a combined effect of long range dispersal and reproductive maturity period as follows.

At very earlier times (less than t_m) the spatial spread develops a single patch, surrounded by several isolated individuals, with a broad distribution of distances to the parental, some of them very large. When those individuals reach the maturity they form secondary foci that begin to grow in almost isolated areas, reproducing the growing structure of the main patch. In the mean time, the main patch continues growing. Now, the invasion front for species with long range dispersal is expected to grow exponentially with time instead of having a constant velocity [9]. That means, the older the patch the faster its growth and therefore the main patch absorbs the secondary patches that are located near it, at early times after their generation. Hence, the global pattern that results from this process is composed by a rather compact main patch with a complicated border structure, surrounded by patches with a broad distribution of sizes. Similar patterns have been observed in a correlated percolation model with long range correlations for urban growth [14]. We will concentrate now in the structure of the main patch border (see section Methods for details of patch and border extraction algorithms details).

Since the patches that are absorbed by the main patch have its same structure on the average, the border develops a self-similar structure, as can be seen in Fig. 2. To characterize such structure
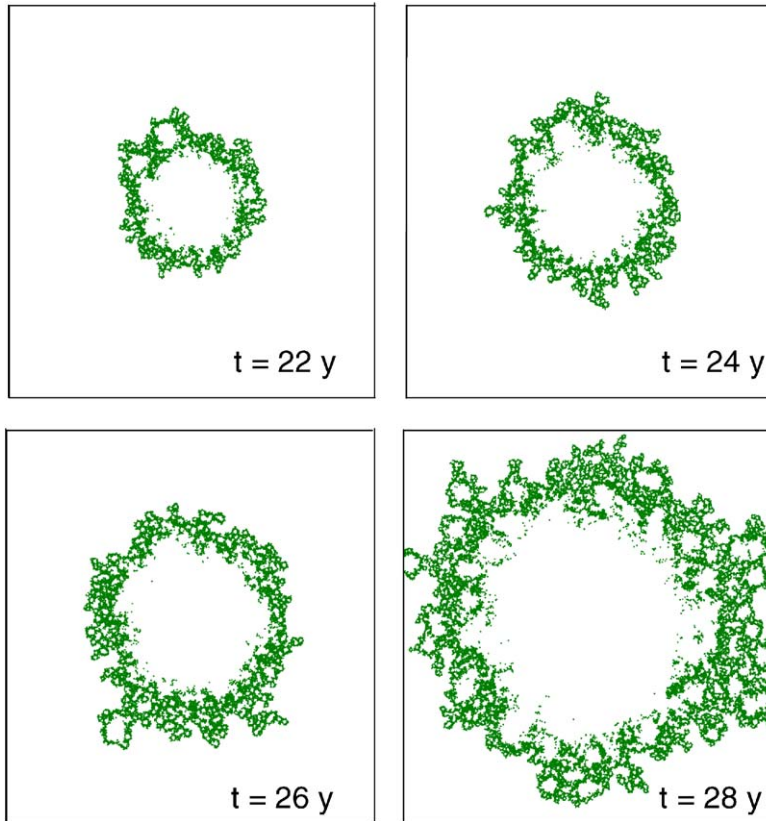
Fig. 2. Snapshots of the main patch border in a square area with $L = 1024$, $d = 5$ ($\alpha = 3.11$) and $t_m = 7$, at different times between two reproductive periods. Notice the sudden growth at $t = 28$, which results from the absorption of the patches associated with secondary foci (not shown; the distribution of those patches can be seen in Fig. 1(b)).

we calculated the mean fractal dimension D of the border as a function of time, where the averages are taken at fixed times over several simulation runs. To calculate D we used a box counting algorithm [13]. That is, we calculate the number of boxes $N(l)$ of linear size l as a function of l; the fractal dimension is then defined through the relation $N(l) \propto l^D$. In Fig. 3 we plot D vs. time for $t_m = 7$ and different values of α in a $L = 1024$ grid. Every curve D vs. t is averaged over 20 independent simulation runs. We observe that statistical fluctuations become very large as α decreases. Some estimation checks performed by averaging over 100 simulation runs indicate that at this number should be increased by least one order of magnitude to reduce significatively the fluctuations, which is out of the present computational capabilities. In a finite system the main patch covers all the area after some finite period and D falls down to one; such characteristic period decreases quickly with α and therefore for the smallest values we can only simulate a very limited time horizon. However, for the largest value of α ($\alpha = 4$) we see that, at long times, D attains an almost stationary regime, where it oscillates around some constant average D_{av} with a time period roughly proportional to t_m. Since we observe the same generation mechanism of the border for every value of α, we can assume the same qualitative behavior for D in all the cases. Moreover,
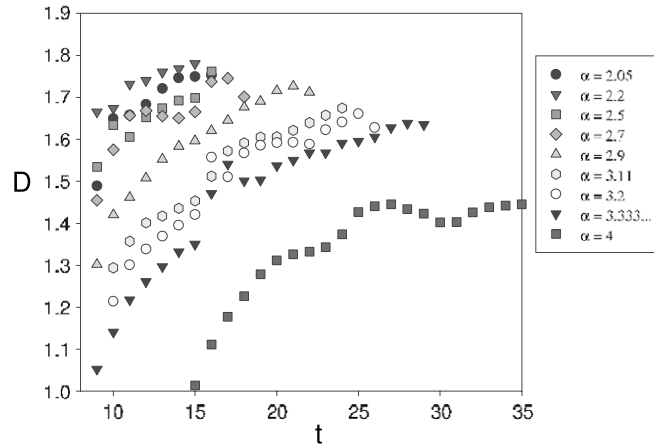
Fig. 3. Mean fractal dimension as a function of time for $L = 1024$, $t_\mathrm{m} = 7$ at different values of α.

the crossover observed between curves corresponding to different values of α suggest that the long term regime has indeed been attained in the time period here considered. We see that the average value D_av increases as α decreases. Such value can be estimated by averaging the values of D over the last six points of every curve (which corresponds approximately to the period of oscillation observed for $\alpha = 4$). In Fig. 4 we show D_av as a function of α. We can clearly distinguish two different regimes: when $2 < \alpha \leqslant 3$ the average fractal dimension appears to be independent of α, with a value that can be roughly estimated as $D_\mathrm{av} = 1.73 \pm 0.03$, while it decreases monotonously with α when $3 < \alpha \leqslant 4$. This type of behavior (stationary properties independent of α when all the moments of the distribution are not defined) is typical of systems with long range interactions and have been observed in several other cellular automata models [15–17]. We also performed some simulations for $t_\mathrm{m} = 10$ and two values of α, to check the influence of t_m the different structures. The mean fractal dimension of the border is compared with the corresponding curves for $t_\mathrm{m} = 7$ in Fig. 5. The results for $\alpha < 3$ suggest that the long term behavior of D is almost insensitive to t_m, while for $\alpha > 3$ there appears to be small dependency on t_m.
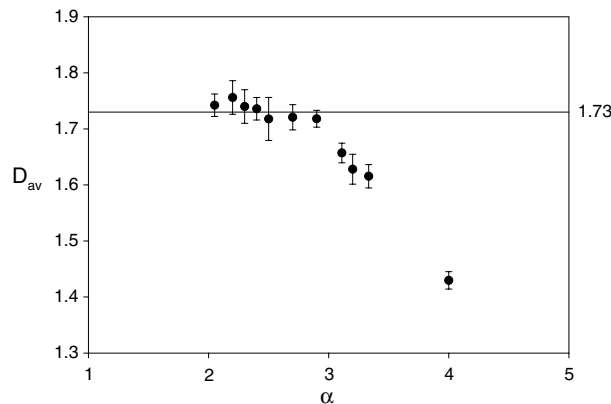

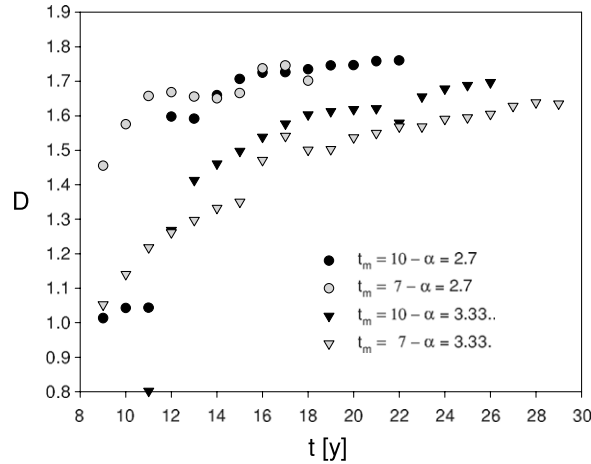Fig. 4. Average fractal dimension at long times as a function of α for $L = 1024$ and $t_\mathrm{m} = 7$.

Fig. 5. Mean fractal dimension as a function of time for $L = 1024$, different values of α and t_{m}.

We next analyze the distribution of secondary patches size, that is, we calculate the relative frequency histogram $P(s)$ of patches with area s (all patches are considered except the main patch) in an area of size $L = 1024$ at intermediate times, that is, for time scales smaller than the characteristic time needed to fill the whole area. Such time scale is determined by tracking the density of occupied sites as a function of the simulation time and is defined as the time below which less than 50% of the sites are occupied; we observed that after this time most of the simulation are is covered by the main patch while the few secondary patches that remain isolated are located near the border and therefore the results are strongly distorted by finite size effects.

We have seen that the fractal dimension of the main patch border exhibit two different types of behavior, according to whether $2 < \alpha \leqslant 3$ or $3 < \alpha \leqslant 4$, so we calculate $P(s)$ for different values of α in both ranges. The results for $P(s)$ are averaged for every value of s and every time step in a sample of M independent runs, M being between 100 and 200. In Fig. 6 we plot $\ln(P(s))$ vs. $\ln(s)$ at different
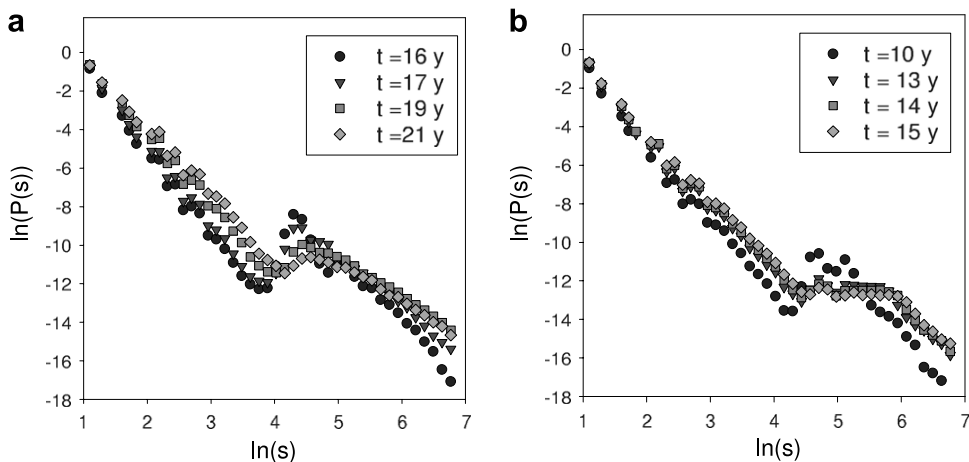

Fig. 6. Log–log plot of the patch sizes distribution $P(s)$ for $L = 1024$ at intermediate times. (a) $\alpha = 3.11\ldots$; (b) $\alpha = 2.7$.

times for $t_m = 7$ and two representative values of α. We see that in both cases $P(s)$ attains at inter-mediate times a stationary distribution, that is, the difference between the values of $P(s)$ at two successive time steps reduces systematically, becoming at the latest stages smaller than statistical fluctuations (estimated a twice the standard deviation from the average) for almost all values of s.

In Fig. 7 we compare the stationary distribution for different values of α. At variance with the fractal dimension of the main patch border, we see that the main qualitative features of $P(s)$ appear to be insensitive to the value of α. In all cases $P(s)$ exhibit two different power laws $P(s) \sim s^{-\beta}$ (evidenced by straight lines in the log–log plot) at small and large spatial scales. The slopes in Fig. 7 are estimated by separating, for every value of α, the points in two sets corresponding to the small and large scales regimes, by eliminating the points in the crossover region (large pronounced kink for $\alpha > 3$ and an almost flat region for $\alpha < 3$); both sets are fitted with a linear regression, giving exponents β ranging between -3.7 and -3.9 in the small scale region and β between -1.9 and -2.1 in the large scale region ($R^2 > 0.98$ in all the cases). Such variation with α is smaller than the error bars in the estimation of the slopes in all the cases. Hence, we see that the exponents of the power laws appear to be almost insensitive to the dispersal range exponent α, the only appreciable effect being a change in the position and the width of the crossover range between the two power laws.

Now this type of distribution of patch sizes is a combined effect of random colonization with a probability distribution Eq. (4) from the different seed source points and the generation of large patches from secondary foci of dispersal resulting from those individuals that reach the maturity. In the last case each patch is composed by descents of the same founder parent located at the corresponding focus.

To discriminate between the effects associated with both causes we repeated the simulations without descent reproduction, i.e., taking $t_m = \infty$ for all individuals except the original parent. This represents the spread from a single mature individual when the reproductive period is much longer than the observation time. In this case all patches but the main one (that is, the patch surrounding the unique focus) are created by random aggregation.

We find that $P(s)$ also develops a stationary state at short and intermediate size scales, characterized by a single power law that extend to larger scales as the observation time increases. Such power law is characterized by an exponent very close to $\beta = -3$, almost independent of the

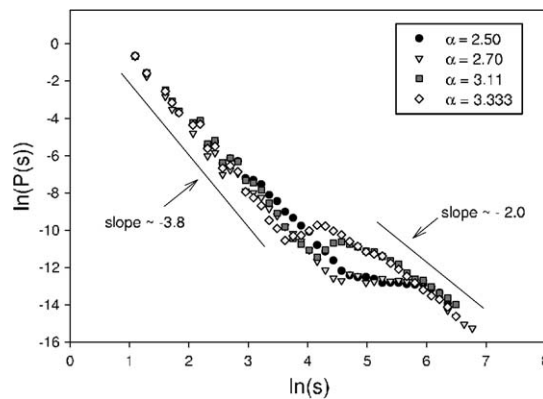
Fig. 7. Comparison of the stationary patch sizes distribution $P(s)$ for $L = 1024$ for different values of α. The straight lines are just for comparison with the average slopes obtained for the small and large scale parts of the distributions.
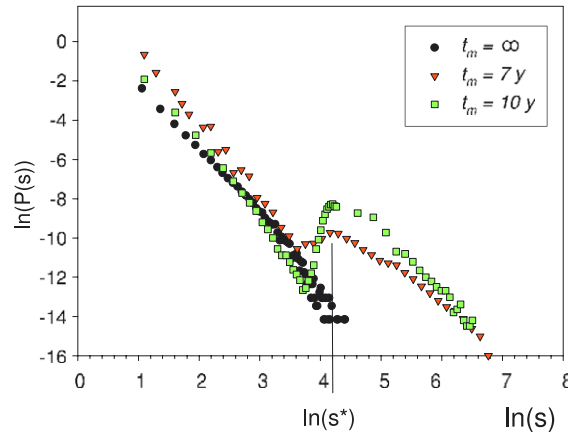
Fig. 8. Stationary patch sizes distribution $P(s)$ for $t_m = 7$ and $t_m = \infty$, for $\alpha = 3.33\ldots$ The tail in the distribution for $t_m = \infty$ converge to the observed power law with exponent $\beta \approx -3$ for small sizes as the observation time increases. $s^* = 65 \pm 5$ ($\ln(s^* \approx 4.2)$)indicates the average minimum size of the patches generated by a single focus for $\alpha = 3.33\ldots$ and finite t_m.

exponent α. An example of the obtained results is shown in Fig. 8, compared with the results for $t_m = 7$ and $t_m = 10$ for the same value of α. We see that the large scale power law and the associated crossover observed for finite t_m is a direct effect of reproduction. Moreover, we calculated the average area s^* of the minimum patch produced by a single focus, that is, the average area of the patch generated by a single individual in its first seed crop. We found that s^* is slightly dependent on α and coincides with the beginning of large scale power law (see Fig. 8). This shows that the large scale power law characterizes the size distribution of patches generated by secondary foci and it appears only for time scales longer than t_m. On the other hand, the small scale power law characterizes the patches generated by random aggregation; the only effect of reproduction in this case is to increase the exponent of the distribution respect to the $t_m = \infty$ case, due to the contribution of secondary foci to the formation of small size patches.

Concerning the effect of t_m on $P(s)$ we observe that the exponent of the small scale power law appears to decrease continuously towards -3 as t_m increases; the large scale behavior for $t_m = 10$ again results consistent with a power law with an exponent which appears to present a slight dependency on t_m ($\beta = -2.3 \pm 0.5$ for $t_m = 10$).

5. Comparison with field data

In this section we compare the simulation predictions with spatial patterns obtained from field data for two different species for which events of LDD appear to be dominant: *C. grandiflora* and *P. ponderosa*. *C. grandiflora* is a non-native shrub, introduced to Australia as an ornamental plant. It was originally planted around the beginning of the 20th century in northern and eastern Queensland, and spread from the original foci was by wind dispersal [21]. The age of reproductive maturity (t_m) is one year [21,23]. *P. ponderosa* is a native pine from the US Rocky Mountains, that have invaded grassland prairies since the mid-1880s [22]. Its seeds are wind dispersed [24] and the age of reproductive maturity (t_m) is seven years.

As can be seen in the vegetation cover map of *C. grandiflora* in Fig. 9, the overall spatial pattern predicted by the simulation (see Fig. 1(b)) appears in a very large spatial scale (hundreds of km, Fig. 9), i.e., a main patch with an irregular border, centered around the focus of the introduction (Charter Towers [21]), surrounded by a distribution of secondary patches. A similar pattern, but in a much smaller spatial scale can be observed in a vegetation cover map for *P. ponderosa* (several km, Fig. 2 in Ref. [22]). This is consistent with the time scale associated with the spread of each species (more than 100 years for *C. grandiflora* [21] and around 30 years for *P. ponderosa* [22]).

In order to obtain a quantitative comparison we first calculate the fractal dimension of the main patch border in both cases. To this end, we digitized both images and isolated the border of all patches. Then we applied the box counting algorithm to the borders, i.e., we calculated the number of boxes needed to cover only the patch border. The fact that all patches present a similar
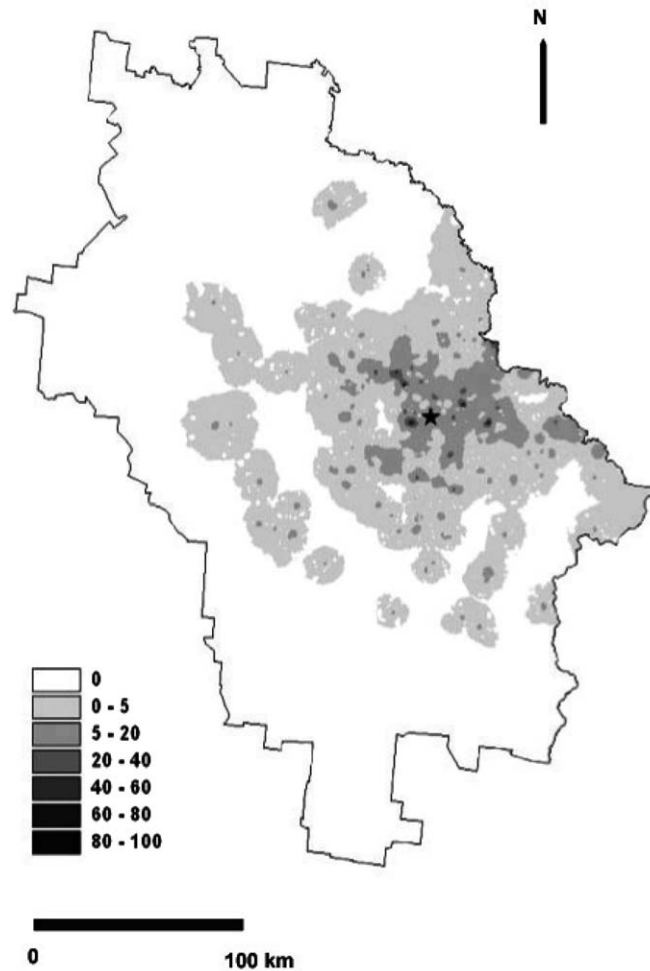

Fig. 9. Abundance (% of cover, derived by Inverse Distance Weighted Interpolation) of *C. grandiflora* in Dalrymple Shire, northern Queensland, Australia (reproduced from Grice et al. [21]). The star indicates the site of first introduction.

border structure allowed us to use all of them in the calculation in order to enhance the statistical sampling. In Fig. 10 we show a log–log plot of the number of boxes of $N(l)$ needed to cover the borders as a function of the linear dimension l. We see that, at large spatial scales, both patterns present a clearly defined fractal dimension $N(l) \sim l^{-D}$, with $D = 1.70 \pm 0.04$ and $D = 1.74 \pm 0.04$, for *C. grandiflora* and *P. ponderosa* respectively; both values are consistent with the prediction of the model for a dispersal distribution function with *infinite mean dispersal distance*, i.e., with an exponent $2 < \alpha \leqslant 3$, or at least for values of α near three, that means a very large mean dispersal distance. The departure from the power law behavior of $N(l)$ at small scales (small l) is expected because such scales correspond to details near the images resolution where diverse scanning effects can distort the spatial pattern.

Next we calculated the distribution of secondary patch sizes $P(s)$ for the case of *P. ponderosa*. The results are shown in Fig. 11. Again, the results are in qualitative (compare with Fig. 7) and quantitative agreement with the prediction of the model, showing a power law behavior at large
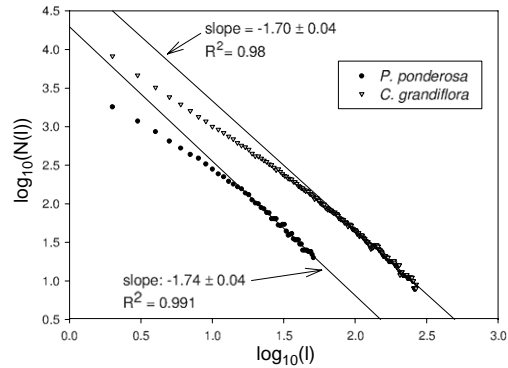

Fig. 10. Log–log plot of number of boxes $N(l)$ of linear dimension l needed to cover patch borders of *C. grandiflora* and *P. ponderosa* as a function of l. R^2 is the correlation coefficient of the linear fittings and l is measured in units of the minimum resolution of the digitized image.
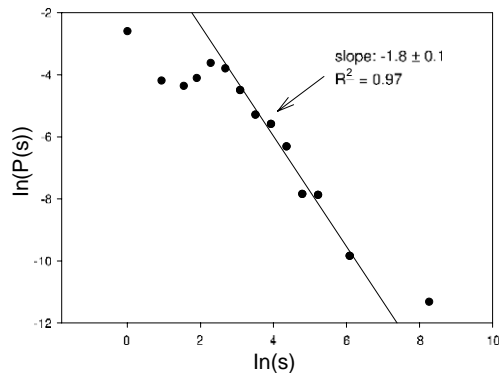

Fig. 11. Log–log plot of the patch sizes distribution $P(s)$ for *P. ponderosa*. The area s is measured in units of the minimum resolution of the digitized image.

spatial scales with an exponent $\beta = 1.8 \pm 0.1$. In the case of *C. grandiflora* the lack of details at relatively small scales in the corresponding image did not allow us to perform a reliable statistical calculation of $P(s)$.

6. Discussion

We showed that the presence of LDD strategies generates distinctive spatial patterns of spread. The main characteristic features of those patterns are some scale-invariant properties for certain temporal scale, during which they become stationary: the fractal character of the main patch and a large scale power law in the patch sizes distribution.

The effect of long-distance dispersal on the spatial pattern for the spread from a single focus predicted by the our model can then summarized as follows. At intermediate time scales, that is, at time scales larger than the characteristic reproductive period of the species, but smaller than the time needed for the covering of the available area, a structured pattern emerges with several stationary properties: a main central patch with a fractal border and a distribution of secondary patches characterized by two different power laws at small and large spatial scales. Both the fractal structure of the main patch and the large scale power law distribution of secondary patches are a combined result of long range dispersal and reproduction. These properties are scale invariant features, that is, one can expect to observe the same type of pattern on very different spatial scales, at least a far as these properties are concerned. Moreover, as time goes these patterns will extend on larger spatial scales, until the available habitat is fulfilled. Hence, the maximum spatial scale on which those effects will be observed is correlated with the time since the introduction of the species in the field. While the large scale part of the size distribution of secondary patches appears to be insensitive to the range of the dispersal (as far as it is long ranged), the fractal dimension of the main patch results very sensitive to the basic statistical structure of the dispersal function: it has an almost constant average (with a value estimated around $D \approx 1.73$) when the dispersal function has no finite moments ($2 < \alpha \leqslant 3$) and smaller values (with a strong dependency on α and t_{m}) when the first moment of the distribution is finite ($3 < \alpha \leqslant 4$). An infinite mean in the basic interactions usually implies mean field behavior [15–18]. This means basically that every individual experiences the same effect from the rest of the system, as if it were interacting with some average environment field. Knowing if a system presents mean field behavior is important because such type of systems present a high degree of universality, that is, one can expect that most of the global properties do not depend on microscopic details, such as heterogeneities in the landscape.

Those features can be detected when the observation time is longer than the reproductive period of the species. While at large scales the power law for the patch sizes distribution appears as a robust feature (i.e., independent of the exponent α of the dispersal distribution and slightly dependent on t_{m}), the fractal dimension of the main patch shows a strong and characteristic dependency on the basic statistical properties of the dispersal distribution, namely, about its second and first moments. Since this quantity can be relatively easily obtained from digitized aerial or satellite images, it appears as a powerful indirect tool to extract statistical features of the basic mechanism of dispersal, either of invasive species or pathogens affecting sessile organisms, like fruitflies or crop fungi. There are also obvious implications for population genetic studies, since LDD events driven by power law distributions of individuals are causing unexpected spatial and temporal

genotypic arrangements. These population and genetic signatures can be easily traced by using the IMCA model together with field remote data.

Acknowledgments

References

[1] R. Petit, E. Pineau, B. Demesure, R. Bacilieri, A. Ducousso, A. Kremer, Chloroplast DNA footprints of postglacial recolonization by oaks, Proc. Natl. Acad. Sci. USA 94 (1997) 996.

[2] A. Cuenca, E. Escalante, D. Piñero, Long-distance colonization,isolation by distance,and historical demography in a relictual Mexican pinyon pine (Pinus nelsonii Shaw) as revealed by paternally inherited genetic markers (cpSSRs), Molecular Ecol. 12 (2003) 2087.

[3] J.K.M. Brown, M.S. Hovmoller, Aerial dispersal of pathogens on the global and continental scales and its impact on plant disease, Science 297 (2002) 537.

[4] H. McCallum, D. Harvell, A. Dobson, Rates of spread of marine pathogens, Ecol. Lett. 6 (2003) 1062.

[5] G.M. Ruiz, T.K. Rawlings, F.C. Dobbs, A. Huq, R. Colwell, Global spread of microorganisms by ships, Nature 408 (2000) 49.

[6] M.C. Fisher, G.L. Koenig, T.J. White, G. San-Blas, R. Negroni, I. GutiérrezAlvarez, B. Wanke, J.W. Taylor, Biogeographic range expansion into South America by *Coccidioides immitis* mirrors New World patterns of human migration, PNAS 98 (2001) 4558.

[7] A.V. Suarez, D.A. Holway, T.J. Case, Patterns of spread in biological invasions dominated by long-distance jump dispersal: insights from Argentine ants, PNAS 98 (2001) 1095.

[8] M.W. Shaw, Simulation of population expansion and spatial pattern when individual dispersal distributions do not decline exponentially with distance, Proc. R. Soc. Lond. B 259 (1995) 243.

[9] M. Kot, M.A. Lewis, P. van den Driessche, Dispersal data and the spread of invading organisms, Ecology 77 (1996) 2027.

[10] J.A.N. Filipe, M.M. Maule, Effects of dispersal mechanisms on spatio-temporal development of epidemics, J. Theor. Biol. 226 (2004) 125.

[11] D.E. Marco, S.A. Páez, S.A. Cannas, Species invasiveness in biological invasions: a modelling approach, Biol. Invasions 4 (2002) 193.

[12] S.A. Cannas, D.E. Marco, S.A. Páez, Modelling biological invasions: species traits, species interactions and habitat heterogeneity, Math. Biosci. 183 (2003) 93.

[13] J.F. Gouyet, Physics and Fractal Structures, Springer, 1996.

[14] H.A. Makse, J.S. Andrade Jr., M. Batty, S. Havlin, H.E. Stanley, Modeling urban growth patterns with correlated percolation, Phys. Rev. E 85 (1998) 7054.

[15] S.A. Cannas, Phase diagram of a stochastic cellular automaton with long-range interactions, Physica A 258 (1998) 32.

[16] P.M. Gleiser, F.A. Tamarit, S.A. Cannas, Self-organized criticality in a model of biological evolution with long-range interactions, Physica A 275 (2000) 272.

[17] P.M. Gleiser, S.A. Cannas, F.A. Tamarit, B. Zheng, Long-range effects in granular avalanching, Phys. Rev. E 63 (2001) 042301 (1-4).

[18] S.A. Cannas, A.C.N. de Magalhães, The one-dimensional Potts model with long-range interactions: a renormalization group approach, J. Phys. A: Math. Gen. 30 (1997) 3345.

[19] F. Jeltsch, S.J. Milton, W.R.J. Dean, N. van Rooyen, Analysing shrub encroachment in the southern Kalahari: a grid-based modelling approach, J. Appl. Ecol. 34 (1997) 1497.

[20] P. Alpert, E. Bone, C. Holzapfel, Invasiveness, invasibility and the role of environmental stress in the spread of non-native plants, Perspect. Plant Ecol. Evol. Systemat. 31 (2000) 52.

[21] A.C. Grice, I.J. Radford, B.N. Abbott, Regional and landscape-scale patterns of shrub invasion in tropical savannas, Biol. Invasions 2 (2000) 187.

[22] J.N. Mast, T.T. Veblen, M.E. Hodgson, Tree invasion within a pine/grassland ecotone: an approach with historic aerial photography and GIS modeling, Forest Ecol. Manage. 93 (1997) 181.

[23] http://www.ento.csiro.au/research/pestmgmt/IPMModellingNetwork/rubbervine.htm.

[24] W.W. Oliver, R.A. Ryker, *Pinus ponderosa* Dougl. ex Laws. ponderosa pine, in: M.R. Burns, B.H. Honkala, technical coordinators, Silvics of North America. Volume 1. Conifers. Agric. Handb. 654, 1990, US Department of Agriculture, Forest Service, Washington, DC, p. 413.